
APEX: PROBING NEURAL NETWORKS VIA ACTIVATION PERTURBATION

REN Tao
 Aalborg University
 Denmark
 taoren@es.aau.dk

Xiaoyu Luo
 Aalborg University
 Denmark
 xilu@cs.aau.dk

Qiongxu Li
 Aalborg University
 Denmark
 qili@es.aau.dk

ABSTRACT

Prior work on probing neural networks primarily relies on input-space analysis or parameter perturbation, both of which face fundamental limitations in accessing structural information encoded in intermediate representations. We introduce **A**ctivation **P**erturbation for **E**Xploration (APEX), an inference-time probing paradigm that perturbs hidden activations while keeping both inputs and model parameters fixed. We theoretically show that activation perturbation induces a principled transition from sample-dependent to model-dependent behavior by suppressing input-specific signals and amplifying representation-level structure, and further establish that input perturbation corresponds to a constrained special case of this framework. Through representative case studies, we demonstrate the practical advantages of APEX. In the small-noise regime, APEX provides a lightweight and efficient measure of sample regularity that aligns with established metrics, while also distinguishing structured from randomly labeled models and revealing semantically coherent prediction transitions. In the large-noise regime, APEX exposes training-induced model-level biases, including a pronounced concentration of predictions on the target class in backdoored models. Overall, our results show that APEX offers an effective perspective for exploring, and understanding neural networks beyond what is accessible from input space alone.

1 Introduction

Characterizing the information encoded in neural networks remains a central challenge in modern machine learning. Although training is driven by input–output supervision, a trained model ultimately operates through a hierarchy of hidden representations that mediate between data and prediction, encoding biases induced by the training data and regime Liu et al. [2020], Li et al. [2025], Srivastava et al. [2024]. As a result, phenomena such as generalization, memorization, robustness, and security vulnerabilities are fundamentally representation-level effects rather than purely input–output properties Li et al. [2018], Tishby and Zaslavsky [2015]. A central goal of model analysis is therefore to characterize how information is organized within this hidden representation space.

A common approach to probing models is to analyze their responses to perturbations on inputs or parameters Ivanovs et al. [2021]. Input perturbations have been used to study robustness and decision boundaries, while parameter perturbations are employed to assess model sensitivity Fawzi et al. [2016], Karimi and Derr [2022], Davis et al. [2021], Sharma et al. [2024]. However, input-space perturbations must propagate through successive nonlinear transformations and can only induce variations that lie within the image of the input-to-representation mapping Feng et al. [2022], rendering large portions of the internal representation space unreachable. Parameter perturbations alter the model itself, entangling the probing signal with changes to the object under study. Consequently, existing probing frameworks that operate through input or parameter perturbations may provide an incomplete view of the information encoded in internal representations.

To address this gap, we introduce Activation Perturbation for EXploration (APEX), an inference-time probing paradigm that perturbs hidden activations while keeping both inputs and parameters fixed. This design enables direct access to intermediate representations beyond the constraints imposed by input-space reachability. We show that input

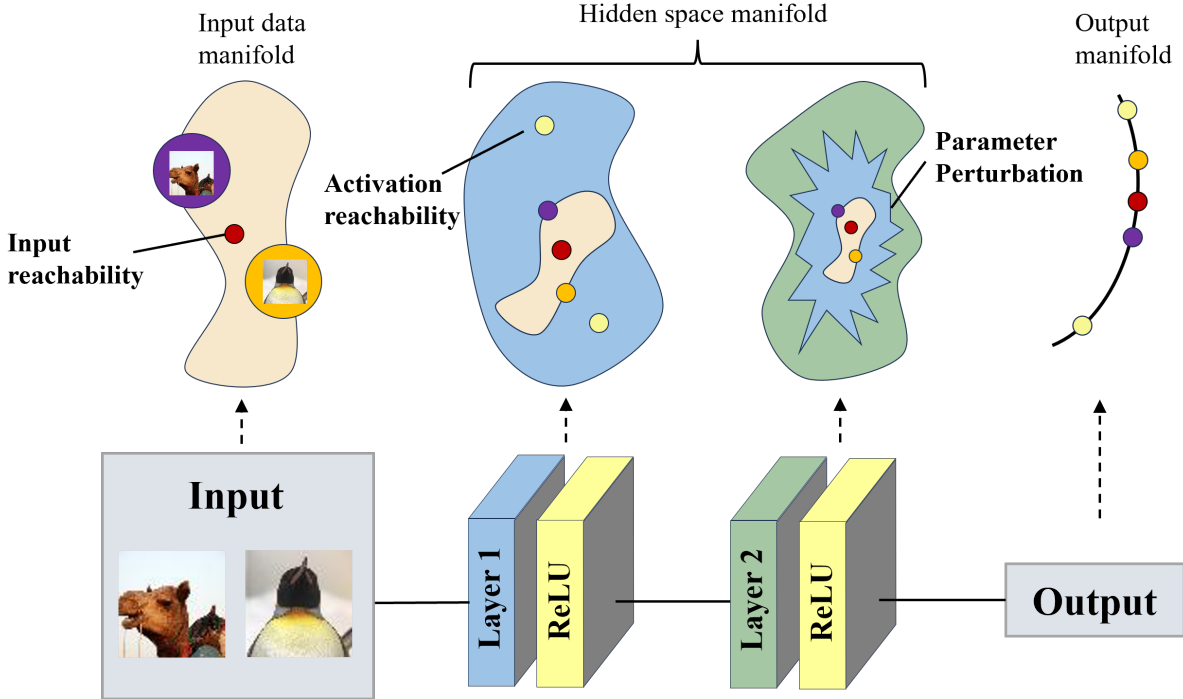


Figure 1: Conceptual illustration of probing mechanisms. Input perturbations are constrained by input-to-representation mapping, parameter perturbations modify the model itself, whereas **APEX** operates directly on hidden representations, enabling exploration beyond input reachability without modifying model parameters.

perturbation can be interpreted as a constrained special case of APEX, yielding a unified structural perspective on existing probing mechanisms. We further show that increasing activation noise induces a transition from sample-dependent to model-dependent behavior, revealing both local, instance-specific structure and global, model-level organization, which is analyzed in detail in Section 3. Figure 1 illustrates the conceptual differences among these probing paradigms.

Consistent with this interpretation, APEX reveals two recurring empirical regimes that reflect how information is organized within learned representations. In the small-noise regime, APEX provides a lightweight and efficient measure of sample regularity that aligns with established metrics, while also distinguishing models trained on structured versus randomly labeled data, and in controlled settings reveals prediction transitions that are consistent with semantic structure learned by the model. In the large-noise regime, predictions become input-independent and converge to a stationary, model-specific output distribution, exposing training-induced model-level biases, including a pronounced concentration of probability mass on the target class in backdoored models. Together, these observations indicate that APEX can expose representation-level structure in a more semantically aligned manner in our controlled experiments, whereas input- and parameter-level perturbations do not exhibit the same behavior under these settings. Our contributions are:

- We provide evidence that perturbing hidden activations yields more semantically aligned probing behavior under controlled conditions, compared to input- or parameter-level perturbations.
- We demonstrate that activation perturbation reveals a unified two-regime behavior: under small noise, prediction stability is correlated with sample-level regularity, while under large noise, output distributions become input-agnostic and reflect model-level structure, including imprints of the training data.
- We show that the stationary output distribution induced by large activation noise encodes intrinsic model biases. In particular, backdoored models exhibit target-aligned concentration in this regime, whereas benign models produce more dispersed outputs, a distinction that is difficult to be revealed by input- or parameter-level perturbations.

2 Related work

Sample Regularity and Memorization Prior work has shown that not all training samples are treated equally by deep networks. Long-tailed or atypical samples tend to be memorized Li et al. [2025], while representative samples

generalize more robustly Feldman [2020]. Several metrics have been proposed to quantify this notion of *sample regularity*, including memorization-based scores Feldman and Zhang [2020] and consistency-based measures Jiang et al. [2021]. Despite differences in formulation, these approaches consistently indicate that samples occupy decision regions of varying stability and geometric robustness. Additional discussion is provided in Appendix A.

Backdoor Attacks Backdoor attacks introduce a small fraction of poisoned training samples that cause the trained model to associate a trigger pattern with a target class Li et al. [2024]. While the model behaves normally on clean inputs, the presence of the trigger induces a systematic and input-agnostic prediction shift. Although backdoor mechanisms vary across attack designs Gu et al. [2019], Nguyen and Tran [2020], Doan et al. [2021], their common effect is to embed a persistent structural bias toward the target class within the model’s internal representations.

Perturbation-Based Probing. A common approach to probing neural networks is through input perturbations, which relate robustness to local decision geometry. For example, Fawzi et al. [2018] analyze model responses to random and structured perturbations constrained to low-dimensional subspaces, showing that the minimal perturbation norm reflects the distance and curvature of the decision boundary. Karimi and Derr [2022] further study local decision structure by generating perturbations near class boundaries and examining the behavior of borderline samples. Another line of work probes models via parameter perturbations. Sharma et al. [2024] quantify sensitivity by measuring expected changes in activations and gradients under random weight perturbations, and use this metric to analyze model stability and guide architecture design.

Recent work has shown that injecting noise into hidden activations at inference time can degrade safety guardrails in large language models Shahani et al. [2025], indicating that activation-level perturbations can meaningfully affect model behavior. This observation highlights the potential of activation perturbation as a probe of internal model structure.

3 Activation Perturbation Framework

We now proceed to explain details of the proposed **APEX**, a simple yet effective framework for analyzing neural network behavior by introducing controlled stochastic perturbations into intermediate activations and observing the resulting output variations. The core idea of APEX is to probe the internal sensitivity and response patterns of a trained model without modifying its parameters or input data, thereby enabling direct exploration of internal representation space beyond input reachability. Despite its conceptual simplicity, this approach enables systematic characterization of prediction stability and reveals abnormal behaviors that are difficult to capture through standard approaches such as input and parameter perturbations.

Formally, consider an L -layer neural network $f_\theta : \mathbb{R}^d \rightarrow \mathbb{R}^c$ with layer-wise transformations

$$z_\ell = W_\ell a_{\ell-1} + b_\ell, \quad a_\ell = \phi(z_\ell),$$

where W_ℓ and b_ℓ are the weight matrix and bias term of layer ℓ , and $\phi(\cdot)$ is the activation function, so that z_ℓ and $a_\ell = \phi(z_\ell)$ denote the pre- and post-activation representations, respectively. To probe the structure and sensitivity of internal representations in a trained model, we perform repeated forward passes while injecting Gaussian noise after each activation:

$$\tilde{a}_\ell = \phi(z_\ell) + \sigma \xi_\ell, \quad \xi_\ell \sim \mathcal{N}(0, I).$$

Here, ξ_ℓ denotes a Gaussian noise vector with i.i.d. entries, and σ is a positive scaling factor controlling the perturbation magnitude. The input x , model parameters θ , and pre-activations z_ℓ remain fixed across runs. Noise realizations are independently drawn across layers and repetitions.

3.1 Stochastic Output Distribution Estimation

For a fixed input x and class set \mathcal{Y} , we characterize the model’s predictive behavior under APEX by repeatedly performing stochastic forward passes with injected noise. Specifically, we conduct T independent perturbation trials and record the top-1 predicted class at each run. Let k_t^* denote the predicted class at trial t . We estimate the empirical probability of predicting class k under perturbation magnitude σ as

$$\hat{P}_x(k; \sigma) = \frac{1}{T} \sum_{t=1}^T \mathbf{1}(k_t^* = k), \quad k \in \mathcal{Y}.$$

This sampling-based estimation procedure approximates the output distribution induced by stochastic perturbation.

3.2 Theoretical Characterization of APEX

Activation perturbation does not directly modify the input or the model parameters, yet it reveals both sample-level regularity and model-level structure. Mathematically, it gives rise to a decomposition of the forward signal.

Theorem 3.1 (Decomposition of activation perturbation). *Assume inputs lie in a bounded set $\mathcal{X} = \{x : \|x\| \leq R\}$ under an induced norm $\|\cdot\|$. Then for each layer $\ell \in \{1, \dots, L\}$ there exist a noise-dependent vector v_ℓ , independent of x , and a residual $r_\ell(x; \sigma)$ such that for all $x \in \mathcal{X}$ and $\sigma > 0$,*

$$\tilde{a}_\ell(x; \sigma) = \sigma v_\ell + r_\ell(x; \sigma), \quad \|r_\ell(x; \sigma)\| \leq B_\ell(R; W, b), \quad (1)$$

where $B_\ell(R; W, b)$ is independent of σ . A constructive definition of (v_ℓ, r_ℓ) and the bound are provided in Appendix B and Appendix C.

Applying the decomposition to the final layer yields a corresponding separation at the logits. For $\sigma > 0$, Let $\tilde{a}_L(x; \sigma)$ denote the final hidden activation and $s(x; \sigma) = U\tilde{a}_L(x; \sigma) + c$ the logits. Using $\tilde{a}_L(x; \sigma) = \sigma v_L + r_L(x; \sigma)$, we obtain

$$s(x; \sigma) = \sigma U v_L + \underbrace{(U r_L(x; \sigma) + c)}_{=:e(x; \sigma)}.$$

Thus the predicted class k^* satisfies

$$\arg \max_k s_k(x; \sigma) = \arg \max_k \left((U v_L)_k + \frac{e_k(x; \sigma)}{\sigma} \right).$$

Since $\|e(x; \sigma)\|_\infty \leq \|U\|_\infty B_L(R; W, b) + \|c\|_\infty$ uniformly over $x \in \mathcal{X}$ and $\sigma > 0$ (Appendix C), the input-dependent term $e(x; \sigma)/\sigma$ vanishes as σ grows. Consequently, the prediction becomes increasingly governed (in distribution) by the model-induced random logits $U v_L$ rather than the specific input x . More precisely, conditioning on a fixed noise draw, once σ exceeds a margin-based threshold, the predicted label becomes independent of x ; under noise resampling at inference time, this implies that the prediction distribution converges to a model-specific limit (Appendix D).

When $\sigma = 0$, the network reduces to its standard deterministic form and the output is entirely determined by the unperturbed activations. For $\sigma > 0$, the decomposition induces two regimes:

Small-noise regime: When σ is small, the residual term dominates, and the perturbed network behaves similarly to the original deterministic model; its output remains sensitive to the input sample.

Large-noise regime: When σ is large, the σv_ℓ component dominates and the prediction becomes increasingly insensitive to the input (in distribution). Appendix D formalizes the corresponding stationary, model-specific prediction distribution.

Input perturbation as a special case. Input samples play a central role in shaping the geometry and decision boundaries of neural networks, reflecting a close connection between data distributions and learned representations Karimi and Derr [2022], Fawzi et al. [2018, 2016]. From a functional perspective, input perturbation can be viewed as a special case of activation perturbation. Perturbing the input x by ε induces a corresponding perturbation at any intermediate layer ℓ ,

$$a_\ell(x + \varepsilon) = a_\ell(x) + \Delta_\ell(x, \varepsilon),$$

where $\Delta_\ell(x, \varepsilon) := a_\ell(x + \varepsilon) - a_\ell(x)$, is entirely determined by the prefix network up to layer ℓ . Thus, input perturbation amounts to injecting a *constrained* perturbation into the activation space, followed by the same suffix network. Taking $\ell = 0$ recovers the input layer itself, making input noise a degenerate instance of activation noise.

For small ε , a first-order expansion yields $\Delta_\ell(x, \varepsilon) \approx J_{a_\ell}(x)\varepsilon$, where $J_{a_\ell}(x)$ denotes the Jacobian of the prefix network Novak et al. [2018], Liu et al. [2024]. Consequently, input perturbations can only induce activation changes lying in the image of this Jacobian, which typically forms a highly constrained subset of the representation space Feng et al. [2022].

Together, this analysis explains why APEX separates sample-dependent variability from model-level structure, and why probing at the activation level enables access to representation properties that are fundamentally inaccessible from the input space.

4 Representation Structure under Small Activation Noise

In this section, we study the behavior of APEX in the small-noise regime. Our goal is to examine whether, when sample-dependent structure is preserved, APEX probes internal representations in a manner that is consistent with the

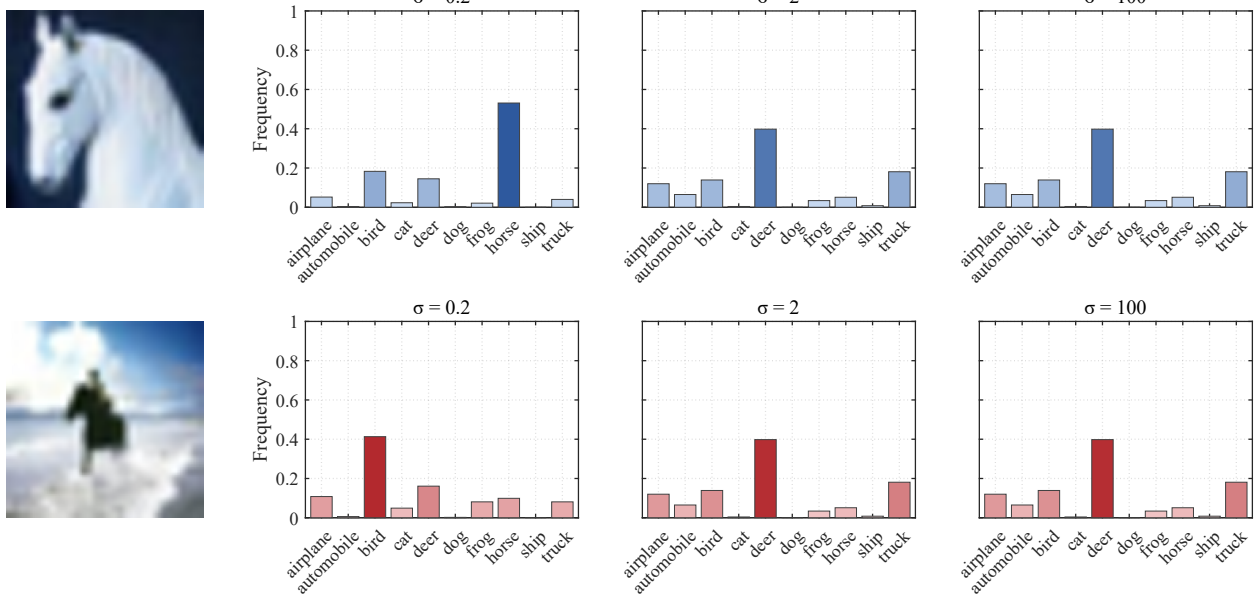


Figure 2: Real examples of the output distributions obtained from two “horse” samples.

semantic structure learned by the model in controlled settings, and whether this behavior differs from that observed under input- or parameter-level perturbations. Detailed experimental setup for following sections is provided in Appendix F.

We begin by illustrating this behavior through a concrete example. Figure 2 shows the output distributions obtained from repeated forward passes of a trained ResNet-18 model on two CIFAR-10 samples under small activation noise. For a typical “horse” image, the predicted class remains dominant across Monte Carlo runs even at $\sigma = 0.2$. In contrast, an atypical “horse” exhibits early prediction shifts toward semantically related classes such as “bird” or “airplane”. These transitions are not arbitrary, but follow semantic proximity in the learned representation space.

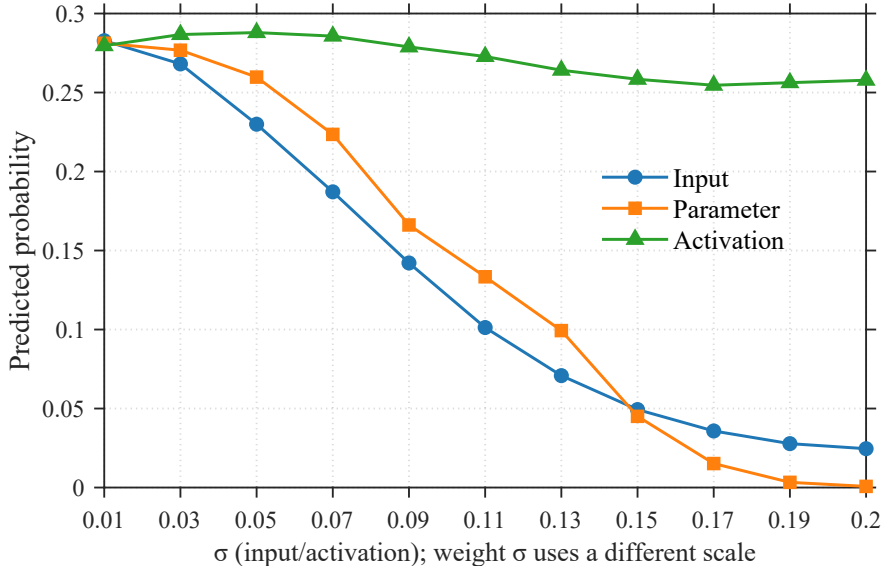


Figure 3: Semantic alignment under small noise. Predicted probability of the reassigned class in a controlled CIFAR-10 setup where two classes share the same input distribution. Only activation perturbation induces a monotonic transfer between the two classes, while input and parameter perturbations do not. (The noise magnitude for weight perturbation is rescaled, and the corresponding σ values equal the x-axis values multiplied by 10^{-1})

4.1 Semantic Alignment of Output Distributions

To directly probe representation-level structure under small activation noise, we design a controlled experiment in which class labels are decoupled from input semantics. Specifically, we construct multiple CIFAR-10 models where two randomly chosen classes share the same underlying input distribution: all original samples from one class are removed, and half of the samples from the other class are randomly reassigned to it. Under this setup, the two classes are semantically indistinguishable, and any preference for one over the other must arise from how the model organizes its internal representations.

In this scenario, a perturbation that faithfully explores the representation space should increasingly transfer samples between the two classes as noise grows. Figure 3 reports the predicted probability of the reassigned class for samples originating from the source class under increasing perturbation strength. While input and parameter perturbations (implementation details in Appendix I) do not exhibit a consistent shift, activation perturbation induces a clear and consistent preference toward the reassigned class. This behavior indicates that, in this controlled setting, activation perturbation induces prediction transitions that are more closely aligned with the representation structure learned by the model, while input- and parameter-level perturbations do not exhibit comparable transitions under the same conditions.

4.2 Revealing Training Imprints

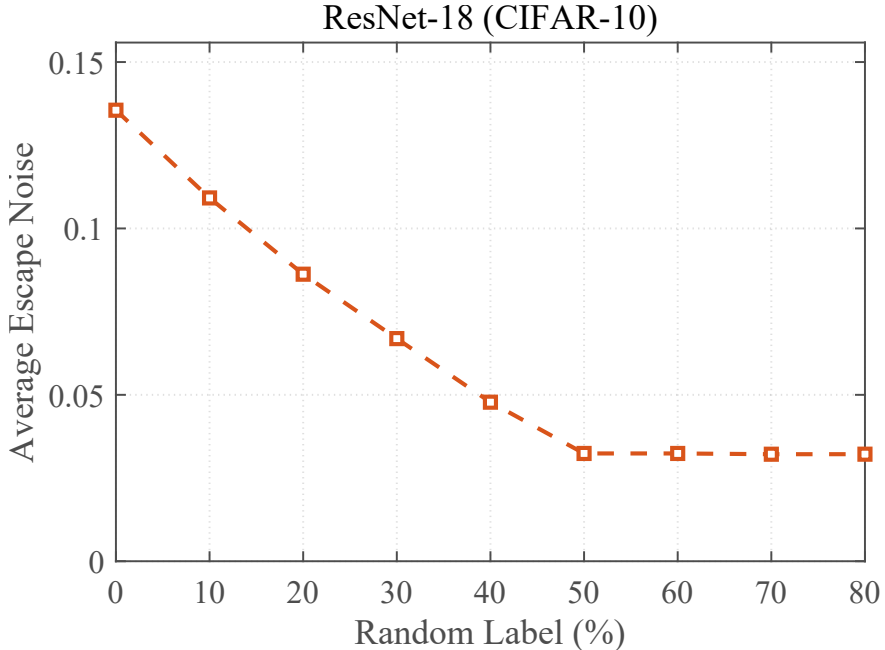


Figure 4: Average escape noise for models with different percentages of samples randomly labeled.

Beyond semantic alignment, we next examine whether APEX can reveal how training distributions shape local representation structure. To this end, we consider models trained on datasets with increasing proportions of randomly assigned labels, a controlled setting known to induce fragmented and irregular decision regions. We examine whether APEX faithfully probes this training-induced fragmentation.

To quantify this effect, we introduce *escape noise* as a scalar descriptor to characterize when a sample’s prediction becomes unstable. Formally, we define the escape noise of a sample as the smallest noise magnitude σ at which the predicted probability of its predicted class k^* drops below a fixed reference level:

$$\hat{P}_x(k^*; \sigma) \leq 0.5. \quad (2)$$

This operational definition provides a convenient way to summarize the relative sensitivity of samples to activation perturbations.

Figure 4 reports results on CIFAR-10 with a ResNet-18 model, showing that the average escape noise decreases monotonically with the random-label ratio. This trend indicates that samples escape their original predictions under much weaker perturbations when local class structure is disrupted. Consistent behavior is observed across additional

dataset–architecture pairs, as reported in Appendix G. This behavior indicates that APEX in the small-noise regime is sensitive to training-induced fragmentation of local representation structure.

By contrast, when the same experiment is conducted with input- or parameter-level perturbations, we do not observe a consistent relationship between perturbation strength and random-label ratio (Appendix H), suggesting that these perturbation sites are less effective at revealing training-induced differences in representation behavior under this setting.

4.3 Connection to Sample-Level Regularity

In the small-noise regime, activation perturbation naturally induces sample-dependent prediction stability, reflecting how individual samples are situated within the learned representation space. This mirrors prior observations that prediction instability under input-level Gaussian perturbations correlates with a sample’s proximity to the decision boundary Fawzi et al. [2016], Gilmer et al. [2019]. Having established that APEX provides a more general probe of representation structure, we briefly examine how its induced stability relates to established notions of sample-level regularity.

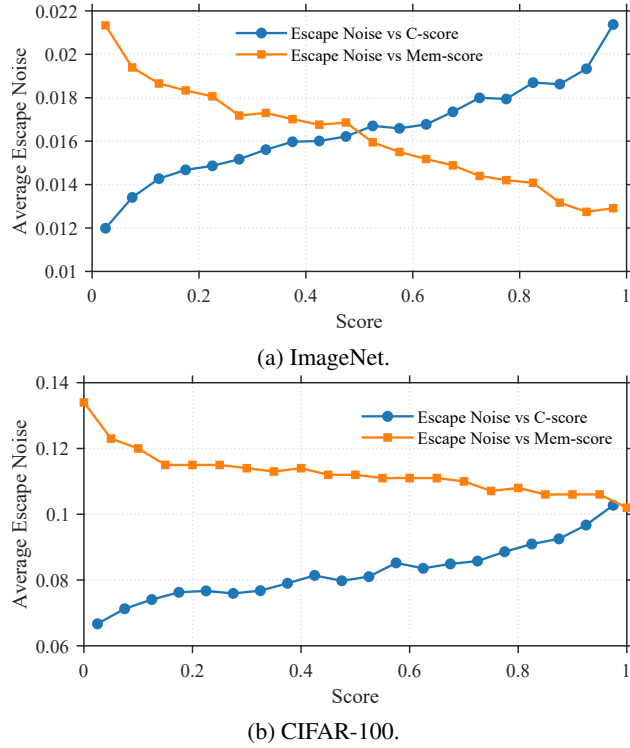


Figure 5: Relationship between average escape noise and memorization score (Mem-score), consistency score (C-score) on ImageNet and CIFAR-100.

Alignment with Established Regularity Measures.

We compare escape noise with established sample regularity metrics, including memorization score Feldman [2020], Feldman and Zhang [2020] and consistency score Jiang et al. [2021]. As shown in Figure 5, escape noise exhibits strong correlations with both metrics on ImageNet and CIFAR-100 for ResNet-50 models (C-scores for CIFAR-100 follow the Inception-based setting of Jiang et al. [2021]), indicating that prediction stability under small activation noise is broadly consistent with known notions of sample regularity.

Samples with high C-scores and low memorization scores consistently exhibit large escape-noise values, whereas irregular or highly memorized samples escape under substantially smaller perturbations. Similar trends are also observed under input-level noise (Appendix J), confirming that activation perturbation preserves known stability-regularity relationships. Examples are visualized in Figure 6.

Computational Efficiency

The above results suggest that escape noise provides a simple and effective scalar summary of this stability, and can therefore serve as a lightweight metric for quantifying sample-level regularity. Unlike memorization-based metrics

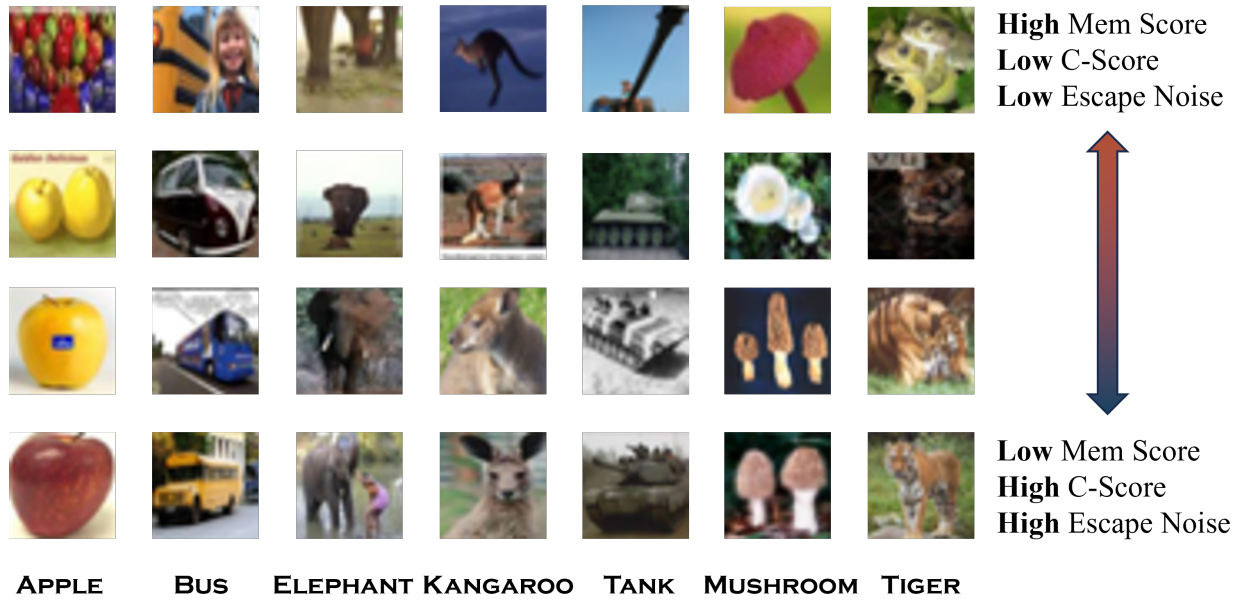


Figure 6: Examples of the regular and irregular samples and their ranges of memorization scores, consistency scores and escape noises.

Feldman [2020], Feldman and Zhang [2020], which require training large ensembles of shadow models, escape noise can be computed using a single trained model with lightweight Monte Carlo inference. This makes it a scalable alternative for large-scale analysis, while remaining consistent with established regularity indicators.

5 Model-Level Stationary Behavior under Large Activation Noise

5.1 Implications of the Large-Noise Regime

The theoretical analysis in Section 3.2 predicts that, as the perturbation magnitude becomes sufficiently large, the noise-driven component dominates the forward signal, causing the network output to become independent of the input sample. This behavior is already hinted at in Figure 2, where the rightmost columns show that, under large noise, the output distributions of different samples become identical.

We verify this prediction quantitatively using a controlled experiment. For a fixed noise magnitude σ , we collect the output distributions obtained from multiple randomly selected input samples and compute the average pairwise JS divergence between them. In addition, for each sample, we measure the JS divergence between its output distributions at consecutive noise levels. As the noise magnitude increases, both quantities rapidly decrease and converge to near-zero values, indicating that (i) output distributions produced from different input samples become identical, and (ii) the distributions stabilize across increasing noise strengths. The results are shown in Appendix K.

Despite this shared sample-independence, the stationary output distributions induced by different perturbation sites exhibit clear qualitative differences. Under input-level perturbations, the stationary output distribution tends to collapse onto a dominant class, suggesting a degenerate form of stationarity. In contrast, activation perturbation yields stationary output distributions that remain substantially more dispersed across classes, indicating a richer and more stable model-level signature. A quantitative comparison based on output entropy is reported in Figure 7.

5.2 Backdoor Models and Target-Aligned Collapse

We next examine whether these stationary output distributions reflect semantically interpretable biases induced in the learned representations during training. Modern deep networks are highly over-parameterized Zhang et al. [2021], and backdoored models are known to devote a disproportionate share of this capacity to their target classes Liu et al. [2018]. Backdoored models provide a particularly suitable testbed, as the induced bias is semantically interpretable and has been shown to be associated with internal representations rather than input-space geometry alone Li et al. [2024], Doan et al. [2021]. To assess whether such target-aligned biases are observable in the stationary output distributions, we

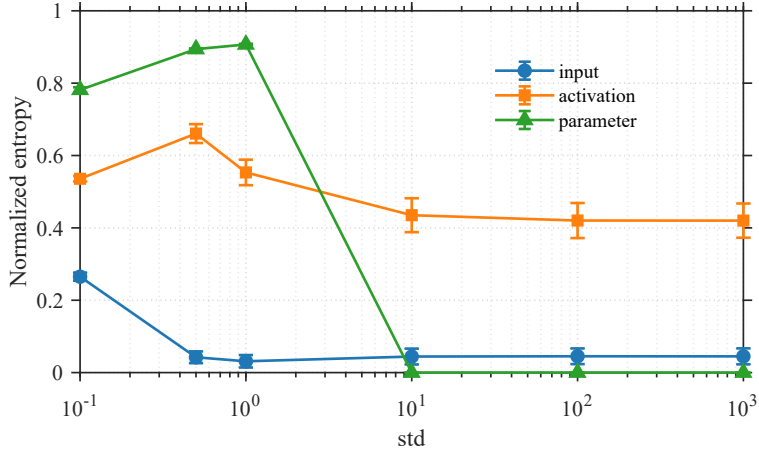


Figure 7: Normalized entropy of output distributions under different σ . Results are averaged over ten Inception models on CIFAR-100.

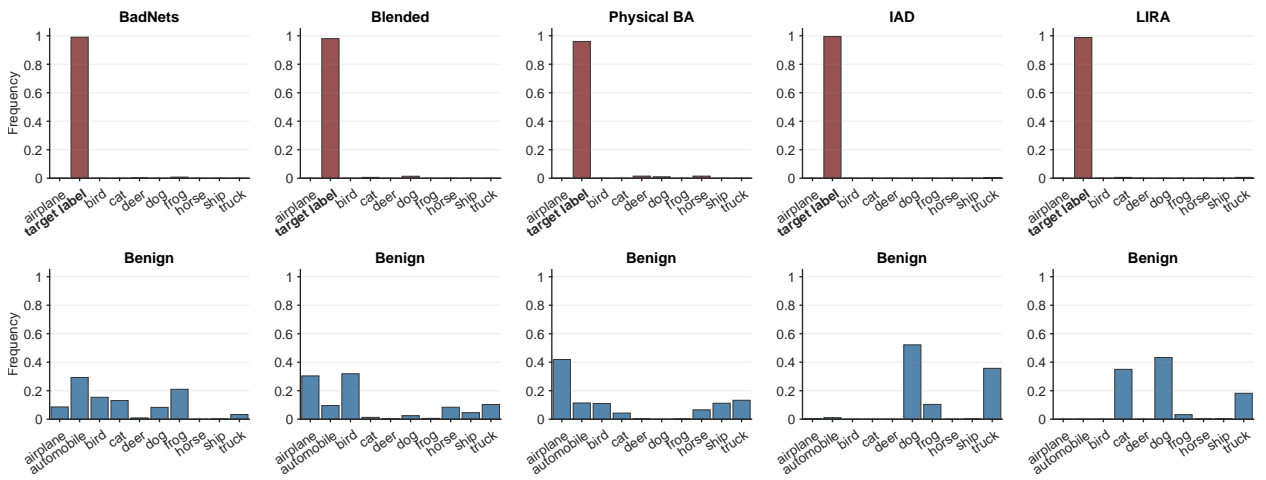


Figure 8: Real examples of model-level distributions for benign and backdoored models under different backdoor attacks: BadNets Gu et al. [2019], Blended Chen et al. [2017], Physical BA Li et al. [2021], IAD Nguyen and Tran [2020] and LIRA Doan et al. [2021].

evaluate APEX across five backdoor attack methods and three network architectures. Representative model-level output distributions are shown in Figure 8.

Probing Backdoor Trigger Bias. For benign models, the stationary output distributions induced by activation perturbation remain broadly spread across multiple classes. In contrast, backdoored models exhibit a pronounced collapse: under sufficiently large activation noise, the vast majority of Monte Carlo runs predict the backdoor target class. More experimental settings are provided in Appendix L. This target-aligned collapse indicates that, once sample-dependent information is removed, the learned representation of a backdoored model is intrinsically biased toward the target class.

This distinction suggests that APEX provides an effective way to expose backdoored model biases. In particular, while optimized input- or parameter-level modifications can be designed or searched to induce target-aligned behavior, simple perturbations at these levels typically do not achieve this effect Wang et al. [2024], Xu et al. [2024]. Although input-level perturbations can also produce sample-independent outputs, their stationary output distributions under non-optimized noise do not concentrate on the backdoor target class (Figure 9).

Figure 10 further shows that benign and backdoored models exhibit systematically different levels of normalized entropy in their stationary output distributions, consistent with the qualitative collapse patterns observed above.

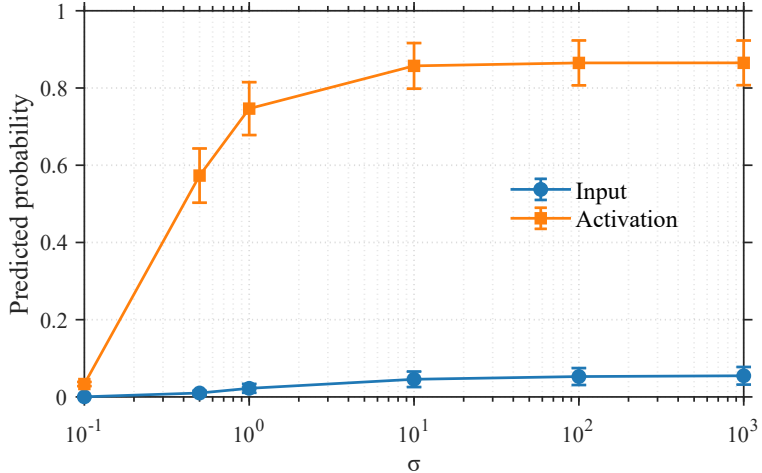


Figure 9: Average predicted probability of the backdoor target class in the model-level output distribution under large perturbations. Results are obtained from ten CIFAR-100 backdoored ResNet-18 models. The probability mass assigned to the target class is averaged across models.

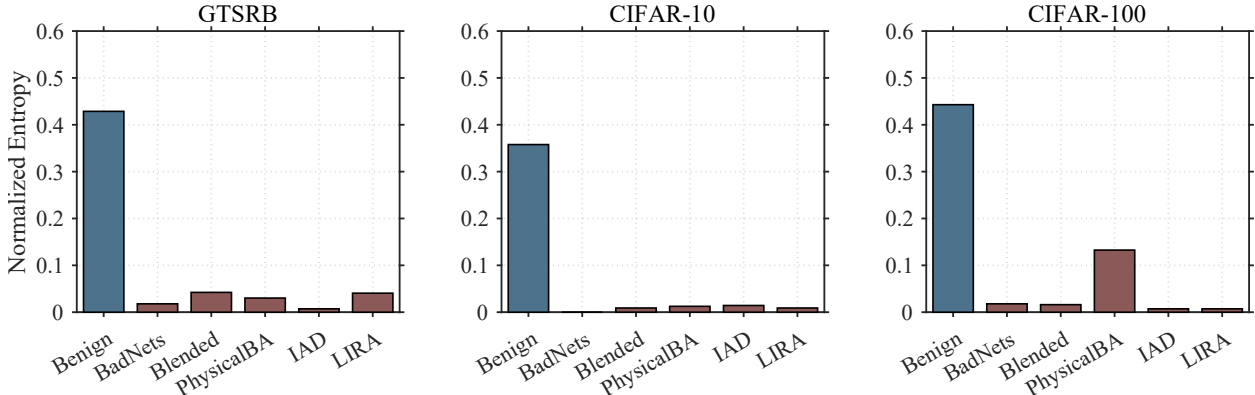


Figure 10: Average normalized entropy of benign and backdoored models across five attacks and three architecture–dataset pairs. Backdoored models consistently show entropy near zero, reflecting highly concentrated distributions.

Effect of Model Capacity. If the stationary output distribution under large activation noise reflects how representation space is allocated across classes, then models with smaller capacity should devote less representational volume to the backdoor target, resulting in weaker collapse and higher output entropy. To test this prediction, we analyze a family of CNNs with increasing depth trained under the same backdoor attack. As shown in Figure 11, deeper models exhibit progressively stronger concentration of probability mass on the target class, while shallower models produce more dispersed stationary distributions. These results suggest that activation perturbation may provide insight into how internal representation space is globally allocated.

Interestingly, the trend is less pronounced in vision transformers (Appendix M). Backdoored DeiT models exhibit partial stationary collapse, with distributions re-dispersing at larger noise levels. This suggests that different architectures may allocate representation space differently, attenuating collapse-based signals in transformers.

6 Robustness Across Probing Configurations

We examine how the behaviors revealed by APEX vary across different probing configurations. These experiments address natural questions about sensitivity to design choices, and help clarify which aspects of the observed phenomena are stable across reasonable variations.

Escape Noise vs. Confidence. We examine whether escape noise merely reflects model confidence accumulated during training. Across training epochs, escape-noise values remain largely unchanged despite a steady increase

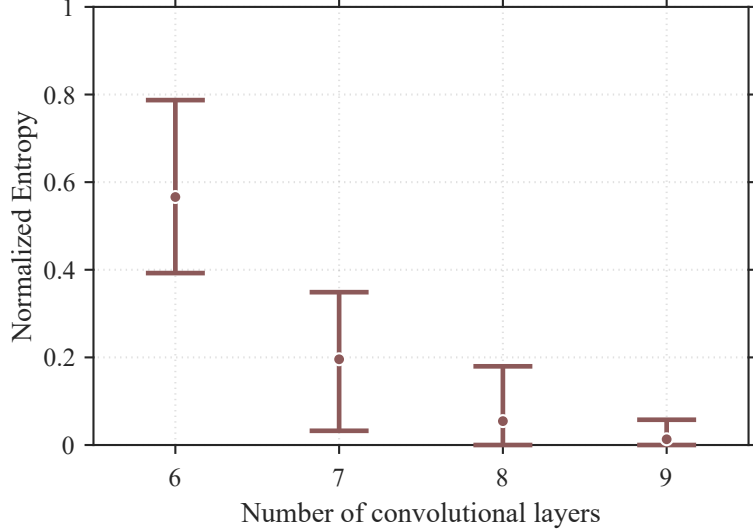


Figure 11: Normalized Entropy of backdoored models under the BadNets attack for X+2Net architectures of varying depth. Deeper models show more concentrated stationary output distributions.

in average softmax confidence, indicating that escape noise is not driven by logit scaling but instead reflects local representation geometry. Detailed results are reported in Appendix N.

Noise Distribution Robustness. We explore whether the stationary output distribution depends on the specific noise distribution used for probing. Gaussian, uniform, and Laplace noise yield nearly identical stationary output distributions (Appendix O), indicating that the effect is not tied to a particular noise model.

Layer-wise Sensitivity. To gain insight into where stationary behavior emerges, we injected noise into individual ReLU layers of both clean and backdoored models and measured the average normalized entropy of the resulting output distributions. Similar to input-level perturbations, layer-wise activation perturbation can also be viewed as a special case of APEX, where noise is injected at a specific depth rather than across all layers. Perturbations to shallow layers produce sharply peaked distributions, whereas perturbations to deeper layers lead to substantially more dispersed outputs (Appendix P).

Activation Function Generality. Finally, we examine whether the observed target-aligned stationary behavior depends on the activation function. Models trained with Leaky ReLU and GELU exhibit the same sharp transition toward the backdoor target as activation noise increases, demonstrating that the stationary behavior arises from the perturbation mechanism itself rather than from ReLU-specific nonlinearities (Appendix Q).

7 Conclusion

We present APEX as a unified inference-time probing paradigm that operates directly in activation space to reveal structural properties of learned representations. By inducing controlled perturbations, APEX exposes a clear behavioral transition from sample-dependent responses to model-dependent dynamics, which can be interpreted as reflecting local representational regularity and global training-induced biases. This unified view connects previously disparate phenomena, including sample regularity estimation, semantic transition analysis, and backdoor-induced target alignment, within a single framework. Together, these results position APEX as a lightweight yet powerful tool for analyzing modern neural networks.

References

Jialun Liu, Yifan Sun, Chuchu Han, Zhaopeng Dou, and Wenhui Li. Deep representation learning on long-tailed data: A learnable embedding augmentation perspective. In *Proceedings of the IEEE/CVF Conference on Computer Vision and Pattern Recognition (CVPR)*, June 2020.

Qiongxiu Li, Xiaoyu Luo, Yiyi Chen, and Johannes Bjerva. Trustworthy machine learning via memorization and the granular long-tail: A survey on interactions, tradeoffs, and beyond, 2025.

Mugdha Srivastava, Abhishek Kaushik, Róisín Loughran, and Kevin McDaid. Data poisoning attacks in the training phase of machine learning models: A review. In *Irish Conference on Artificial Intelligence and Cognitive Science*, 2024.

Chunyuan Li, Heerad Farkhoor, Rosanne Liu, and Jason Yosinski. Measuring the intrinsic dimension of objective landscapes. In *International Conference on Learning Representations*, 2018.

Naftali Tishby and Noga Zaslavsky. Deep learning and the information bottleneck principle. In *2015 IEEE Information Theory Workshop (ITW)*, pages 1–5, 2015. doi: 10.1109/ITW.2015.7133169.

Maksims Ivanovs, Roberts Kadikis, and Kaspars Ozols. Perturbation-based methods for explaining deep neural networks: A survey. *Pattern Recognition Letters*, 150:228–234, 2021. ISSN 0167-8655. doi: <https://doi.org/10.1016/j.patrec.2021.06.030>.

Alhussein Fawzi, Seyed-Mohsen Moosavi-Dezfooli, and Pascal Frossard. Robustness of classifiers: from adversarial to random noise. In *Proceedings of the 30th International Conference on Neural Information Processing Systems, NIPS’16*, page 1632–1640, Red Hook, NY, USA, 2016. Curran Associates Inc. ISBN 9781510838819.

Hamid Karimi and Tyler Derr. Decision boundaries of deep neural networks. In *2022 21st IEEE International Conference on Machine Learning and Applications (ICMLA)*, pages 1085–1092, 2022. doi: 10.1109/ICMLA55696.2022.00179.

Jared Q Davis, Albert Gu, Krzysztof Choromanski, Tri Dao, Christopher Re, Chelsea Finn, and Percy Liang. Catformer: Designing stable transformers via sensitivity analysis. In Marina Meila and Tong Zhang, editors, *Proceedings of the 38th International Conference on Machine Learning*, volume 139 of *Proceedings of Machine Learning Research*, pages 2489–2499. PMLR, 18–24 Jul 2021.

Renu Sharma, Redwan Sony, and Arun Ross. Investigating weight-perturbed deep neural networks with application in iris presentation attack detection. *2024 IEEE/CVF Winter Conference on Applications of Computer Vision Workshops (WACVW)*, pages 1082–1091, 2024.

Ruili Feng, Kecheng Zheng, Yukun Huang, Deli Zhao, Michael Jordan, and Zheng-Jun Zha. Rank diminishing in deep neural networks. In *Proceedings of the 36th International Conference on Neural Information Processing Systems, NIPS ’22*, Red Hook, NY, USA, 2022. Curran Associates Inc. ISBN 9781713871088.

Vitaly Feldman. Does learning require memorization? a short tale about a long tail. In *SIGACT Symposium on Theory of Computing*, pages 954–959. ACM, 2020.

Vitaly Feldman and Chiyuan Zhang. What neural networks memorize and why: Discovering the long tail via influence estimation. In *Advances in Neural Information Processing Systems*, volume 33, pages 2881–2891. Curran Associates, Inc., 2020.

Ziheng Jiang, Chiyuan Zhang, Kunal Talwar, and Michael C Mozer. Characterizing structural regularities of labeled data in overparameterized models. In Marina Meila and Tong Zhang, editors, *Proceedings of the 38th International Conference on Machine Learning*, volume 139 of *Proceedings of Machine Learning Research*, pages 5034–5044. PMLR, 18–24 Jul 2021.

Yiming Li, Yong Jiang, Zhifeng Li, and Shu-Tao Xia. Backdoor learning: A survey. *IEEE Transactions on Neural Networks and Learning Systems*, 35(1):5–22, 2024. doi: 10.1109/TNNLS.2022.3182979.

Tianyu Gu, Kang Liu, Brendan Dolan-Gavitt, and Siddharth Garg. Badnets: Evaluating backdooring attacks on deep neural networks. *IEEE Access*, 7:47230–47244, 2019. doi: 10.1109/ACCESS.2019.2909068.

Tuan Anh Nguyen and Tuan Anh Tran. Input-aware dynamic backdoor attack. In *Proceedings of the 34th International Conference on Neural Information Processing Systems, NIPS ’20*, Red Hook, NY, USA, 2020. Curran Associates Inc. ISBN 9781713829546.

Khoa Doan, Yingjie Lao, Weijie Zhao, and Ping Li. Lira: Learnable, imperceptible and robust backdoor attacks. In *ICCV*, pages 11946–11956, 2021. doi: 10.1109/ICCV48922.2021.01175.

Alhussein Fawzi, Seyed-Mohsen Moosavi-Dezfooli, Pascal Frossard, and Stefano Soatto. Empirical study of the topology and geometry of deep networks. pages 3762–3770, 06 2018. doi: 10.1109/CVPR.2018.00396.

Prithviraj Singh Shahani, Kaveh Eskandari Miandoab, and Matthias Scheutz. Noise injection systemically degrades large language model safety guardrails, 2025.

Roman Novak, Yasaman Bahri, Daniel A. Abolafia, Jeffrey Pennington, and Jascha Sohl-Dickstein. Sensitivity and generalization in neural networks: an empirical study. In *International Conference on Learning Representations*, 2018.

Deyin Liu, Lin Yuanbo Wu, Bo Li, Farid Boussaid, Mohammed Bennamoun, Xianghua Xie, and Chengwu Liang. Jacobian norm with selective input gradient regularization for interpretable adversarial defense. *Pattern Recognition*, 145:109902, 2024. ISSN 0031-3203. doi: <https://doi.org/10.1016/j.patcog.2023.109902>.

Justin Gilmer, Nicolas Ford, Nicholas Carlini, and Ekin Cubuk. Adversarial examples are a natural consequence of test error in noise. In Kamalika Chaudhuri and Ruslan Salakhutdinov, editors, *Proceedings of the 36th International Conference on Machine Learning*, volume 97 of *Proceedings of Machine Learning Research*, pages 2280–2289. PMLR, 09–15 Jun 2019.

Xinyun Chen, Chang Liu, Bo Li, Kimberly Lu, and Dawn Song. Targeted backdoor attacks on deep learning systems using data poisoning, 2017.

Yiming Li, Tongqing Zhai, Yong Jiang, Zhifeng Li, and Shu-Tao Xia. Backdoor attack in the physical world. In *ICLR 2021 Workshop on RobustML*, volume 2104.02361, 2021.

Chiyuan Zhang, Samy Bengio, Moritz Hardt, Benjamin Recht, and Oriol Vinyals. Understanding deep learning (still) requires rethinking generalization. *Commun. ACM*, 64(3):107–115, February 2021. ISSN 0001-0782.

Kang Liu, Brendan Dolan-Gavitt, and Siddharth Garg. Fine-pruning: Defending against backdooring attacks on deep neural networks. In *International symposium on research in attacks, intrusions, and defenses*, pages 273–294. Springer, 2018.

Hang Wang, Zhen Xiang, David J. Miller, and George Kesisidis. MM-BD: Post-Training Detection of Backdoor Attacks with Arbitrary Backdoor Pattern Types Using a Maximum Margin Statistic. In *2024 IEEE Symposium on Security and Privacy (SP)*, pages 1994–2012, Los Alamitos, CA, USA, May 2024. IEEE Computer Society. doi: 10.1109/SP54263.2024.00015. URL <https://doi.ieee.org/10.1109/SP54263.2024.00015>.

Xiaoyun Xu, Zhuoran Liu, Stefanos Koffas, Shujian Yu, and Stjepan Picek. BAN: Detecting backdoors activated by neuron noise. In *The Thirty-eighth Annual Conference on Neural Information Processing Systems*, 2024. URL <https://openreview.net/forum?id=asYYSzL4N5>.

Hongyan Chang and Reza Shokri. On the privacy risks of algorithmic fairness. pages 292–303. IEEE, 2021.

Isha Garg, Deepak Ravikumar, and Kaushik Roy. Memorization through the lens of curvature of loss function around samples. *arXiv preprint arXiv:2307.05831*, 2023.

Daniel D’souza, Zach Nussbaum, Chirag Agarwal, and Sara Hooker. A tale of two long tails. *arXiv preprint arXiv:2107.13098*, 2021.

A. et al. Krizhevsky. Learning multiple layers of features from tiny images. In *Univ. Toronto Tech. Rep.*, 2009.

J. et al. Stallkamp. The german traffic sign recognition benchmark: A multi-class classification competition. In *IEEE IJCNN*, pages 1453–1460, 2011.

Olga Russakovsky, Jia Deng, Hao Su, Jonathan Krause, Sanjeev Satheesh, Sean Ma, Zhiheng Huang, Andrej Karpathy, Aditya Khosla, Michael Bernstein, Alexander C. Berg, and Li Fei-Fei. ImageNet Large Scale Visual Recognition Challenge. *International Journal of Computer Vision (IJCV)*, 115(3):211–252, 2015. doi: 10.1007/s11263-015-0816-y.

K. et al. He. Deep residual learning for image recognition. In *Proc. CVPR*, pages 770–778, 2016.

Karen Simonyan and Andrew Zisserman. Very deep convolutional networks for large-scale image recognition. In *International Conference on Learning Representations*, 2015.

Gao Huang, Zhuang Liu, Laurens Van Der Maaten, and Kilian Q. Weinberger. Densely connected convolutional networks. In *2017 IEEE Conference on Computer Vision and Pattern Recognition (CVPR)*, pages 2261–2269, 2017. doi: 10.1109/CVPR.2017.243.

Yiming Li, Mengxi Ya, Yang Bai, Yong Jiang, and Shu-Tao Xia. Backdoorbox: A python toolbox for backdoor learning. In *ICLR 2023 Workshop on Backdoor Attacks and Defenses in Machine Learning*, 2023. *arXiv:2302.01762*.

A Memorization and long-tailed distribution

Beyond its impact on generation performance, memorization in deep neural networks has far-reaching implications for safety and security considerations, including privacy leakage and fairness disparities Feldman [2020], Chang and Shokri [2021], Garg et al. [2023].

The memorization score Feldman and Zhang [2020] measures the extent to which a trained model's prediction on a particular example depends on whether that example was included during training. Let \mathcal{A} be a (possibly randomized) learning algorithm and D_{tr} a training set. For an example $i = (x_i, y_i) \in D_{\text{tr}}$, its (label) memorization score is defined via a leave-one-out comparison:

$$\text{mem}(\mathcal{A}, D_{\text{tr}}, i) = \Pr_{h \leftarrow \mathcal{A}(D_{\text{tr}})} [h(x_i) = y_i] - \Pr_{h \leftarrow \mathcal{A}(D_{\text{tr}} \setminus \{i\})} [h(x_i) = y_i], \quad (3)$$

where $D_{\text{tr}} \setminus \{i\}$ denotes the dataset obtained by removing i from D_{tr} .

Intuitively, $\text{mem}(\cdot)$ captures the marginal influence of a single training point on the model's correctness at that point. A larger value indicates that the model relies more heavily on i to predict y_i , which is commonly interpreted as a signal of elevated privacy exposure since the model's behavior changes noticeably when i is present versus absent. Empirically, high memorization scores tend to concentrate on atypical or hard-to-learn instances, whereas low scores are more often associated with typical, easy examples across datasets Feldman and Zhang [2020], aligning with qualitative notions of example difficulty. D'souza et al. [2021] showing that the long tail itself is heterogeneous: atypical-but-valid samples correspond to reducible (epistemic) uncertainty, whereas noisy samples induce irreducible (aleatoric) uncertainty and exhibit distinct learning dynamics. A recent survey echoes that conflating these different sources of tail behavior obscures the interpretation of memorization, whose implications for generalization, privacy, and robustness depend critically on whether memorization arises from atypicality or noise Li et al. [2025].

B Decomposition of Activation-Perturbed Activations

We detail the layerwise decomposition used in Theorem 3.1.

Decomposition after ReLU with uniformly bounded residual. Assume noise is added after each ReLU:

$$\begin{aligned} \tilde{a}_1(x; \sigma) &= \text{ReLU}(W_1 x + b_1) + \sigma \xi_1, \\ \tilde{a}_\ell(x; \sigma) &= \text{ReLU}(W_\ell \tilde{a}_{\ell-1}(x; \sigma) + b_\ell) + \sigma \xi_\ell, \quad \ell = 2, \dots, L. \end{aligned}$$

We show by induction that for each ℓ there exist v_ℓ (depending on (W, b, ξ) but not on x) and $r_\ell(x; \sigma)$ such that

$$\tilde{a}_\ell(x; \sigma) = \sigma v_\ell + r_\ell(x; \sigma), \quad \|r_\ell(x; \sigma)\| \leq B_\ell(R; W, b),$$

uniformly over $x \in \mathcal{X} = \{x : \|x\| \leq R\}$ and $\sigma > 0$.

Base case ($\ell = 1$). Define

$$v_1 := \xi_1, \quad r_1(x; \sigma) := \text{ReLU}(W_1 x + b_1).$$

Then $\tilde{a}_1(x; \sigma) = \sigma v_1 + r_1(x; \sigma)$ and $\|r_1(x; \sigma)\| \leq \|W_1\|R + \|b_1\|$.

Inductive step. Assume for layer $\ell - 1$ that

$$\tilde{a}_{\ell-1}(x; \sigma) = \sigma v_{\ell-1} + r_{\ell-1}(x; \sigma).$$

Then

$$W_\ell \tilde{a}_{\ell-1}(x; \sigma) + b_\ell = \sigma W_\ell v_{\ell-1} + (W_\ell r_{\ell-1}(x; \sigma) + b_\ell).$$

Applying Lemma E.1 with $a = W_\ell v_{\ell-1}$ and $d = W_\ell r_{\ell-1}(x; \sigma) + b_\ell$, we obtain

$$\text{ReLU}(\sigma W_\ell v_{\ell-1} + W_\ell r_{\ell-1}(x; \sigma) + b_\ell) = \sigma \text{ReLU}(W_\ell v_{\ell-1}) + \Delta_\ell(x; \sigma),$$

where

$$\|\Delta_\ell(x; \sigma)\| \leq \|W_\ell r_{\ell-1}(x; \sigma) + b_\ell\|.$$

Therefore,

$$\tilde{a}_\ell(x; \sigma) = \sigma \text{ReLU}(W_\ell v_{\ell-1}) + \Delta_\ell(x; \sigma) + \sigma \xi_\ell = \sigma v_\ell + r_\ell(x; \sigma),$$

by defining

$$v_\ell := \text{ReLU}(W_\ell v_{\ell-1}) + \xi_\ell, \quad r_\ell(x; \sigma) := \Delta_\ell(x; \sigma).$$

Moreover,

$$\|r_\ell(x; \sigma)\| \leq \|W_\ell r_{\ell-1}(x; \sigma) + b_\ell\| \leq \|W_\ell\| \|r_{\ell-1}(x; \sigma)\| + \|b_\ell\|.$$

Iterating this recursion yields the bound $\|r_\ell(x; \sigma)\| \leq B_\ell(R; W, b)$ from Appendix C, which is independent of σ . \square

C Uniform boundedness of the residual term

Fix an induced operator norm $\|\cdot\|$ and assume inputs lie in a bounded set $\mathcal{X} = \{x : \|x\| \leq R\}$ with $R < \infty$. Let $M_\ell := \|W_\ell\|$ and $b_\ell^* := \|b_\ell\|$. From the inductive step in Appendix B, we have

$$\|r_\ell(x; \sigma)\| \leq \|W_\ell r_{\ell-1}(x; \sigma) + b_\ell\| \leq M_\ell \|r_{\ell-1}(x; \sigma)\| + b_\ell^*.$$

With $r_1(x; \sigma) = \text{ReLU}(W_1 x + b_1)$ and $\|r_1(x; \sigma)\| \leq M_1 R + b_1^*$, recursively we obtain

$$\|r_\ell(x; \sigma)\| \leq B_\ell(R; W, b) := \left(\prod_{j=1}^{\ell} M_j \right) R + \sum_{k=1}^{\ell-1} \left(\prod_{j=k+1}^{\ell} M_j \right) b_k^* + b_\ell^*.$$

Hence $r_\ell(x; \sigma)$ is bounded on \mathcal{X} by $B_\ell(R; W, b)$, which depends on (W, b) and R but is independent of σ .

D Stationary prediction distribution at large noise

We formalize the large-noise regime under noise resampling at inference time.

Write the logits as

$$s(x; \sigma) = U \tilde{a}_L(x; \sigma) + c = \sigma U v_L + e(x; \sigma), \quad e(x; \sigma) := U r_L(x; \sigma) + c.$$

Let $C := \|U\|_\infty B_L(R; W, b) + \|c\|_\infty$, so that $\|e(x; \sigma)\|_\infty \leq C$ for all $x \in \mathcal{X}$ and $\sigma > 0$ (Appendix C).

Conditional stabilization for a fixed noise draw. Condition on a fixed draw of the injected noises (hence a fixed v_L). Let $j^* = \arg \max_i (U v_L)_i$ and define the top-1 margin

$$\delta := (U v_L)_{j^*} - \max_{i \neq j^*} (U v_L)_i.$$

Assume $\delta > 0$. If

$$\sigma > \sigma^* := \frac{2C}{\delta},$$

then for all $x \in \mathcal{X}$,

$$\arg \max_i s_i(x; \sigma) = \arg \max_i (U v_L)_i = j^*.$$

Indeed, for any $i \neq j^*$,

$$s_{j^*}(x; \sigma) - s_i(x; \sigma) = \sigma((U v_L)_{j^*} - (U v_L)_i) + (e_{j^*}(x; \sigma) - e_i(x; \sigma)) \geq \sigma \delta - 2C > 0.$$

Stationary limit under noise resampling. Since noises are resampled at each inference, v_L varies randomly across runs. The previous result implies that as $\sigma \rightarrow \infty$, the prediction distribution converges to the distribution of $\arg \max_i (U v_L)_i$, which depends on the trained model (W, b, U, c) and the noise law, but not on the input x .

E Lemma: ReLU residual bound

Lemma E.1. *For any vectors $a, d \in \mathbb{R}^m$ and scalar $\sigma > 0$, define*

$$\Delta := \text{ReLU}(\sigma a + d) - \sigma \text{ReLU}(a).$$

Then

$$\text{ReLU}(\sigma a + d) = \sigma \text{ReLU}(a) + \Delta, \quad \|\Delta\| \leq \|d\|.$$

Proof. Since ReLU is positively homogeneous for $\alpha \geq 0$, $\text{ReLU}(\sigma a) = \sigma \text{ReLU}(a)$. As ReLU is 1-Lipschitz,

$$\|\text{ReLU}(\sigma a + d) - \text{ReLU}(\sigma a)\| \leq \|d\|.$$

Combining the two identities gives $\|\Delta\| \leq \|d\|$. □

F Experimental Setup

Models and Datasets. We evaluate our method on CIFAR-10, CIFAR-100 Krizhevsky [2009], GTSRB Stallkamp [2011], and ImageNet-1K Russakovsky et al. [2015] using a diverse set of vision architectures. Our experiments cover convolutional models including ResNet-18, ResNet-50 He [2016], VGG-11 Simonyan and Zisserman [2015], DenseNet Huang et al. [2017], Inception, and a family of X+2Net architectures with varying depth, as well as the transformer-based DeiT-Small model. For ImageNet-1K experiments, ResNet-50 is initialized from ImageNet-1K pretrained weights and fine-tuned on the target dataset; all other models and datasets are trained from scratch.

Training Protocol. Unless otherwise stated, all convolutional models are trained using stochastic gradient descent (SGD) with momentum. We adopt a largely unified training configuration across datasets, with minor dataset-specific adjustments. Experiments on CIFAR-10, CIFAR-100, and GTSRB Krizhevsky [2009], Stallkamp [2011] use SGD with momentum 0.9. The following configuration is used:

- Batch size: 256
- Number of dataloader workers: 4
- Learning rate: 0.1
- Weight decay: 5×10^{-4}
- Learning rate scheduler: step decay with milestones at epochs 50 and 80
- Learning rate decay factor: $\gamma = 0.1$
- Total training epochs: 100

Inference-Time Perturbation and Monte Carlo Estimation. All perturbation experiments are conducted strictly at inference time, with model parameters fixed. To estimate the output distribution we perform 1,000 Monte Carlo forward passes per input. For ImageNet-1K, due to computational constraints, we perform 100 Monte Carlo forward passes per input.

G More Results on Random-Label Imprints

Across more settings, increasing label randomness leads to a monotonic decrease in escape noise, indicating progressively fragmented local decision regions.

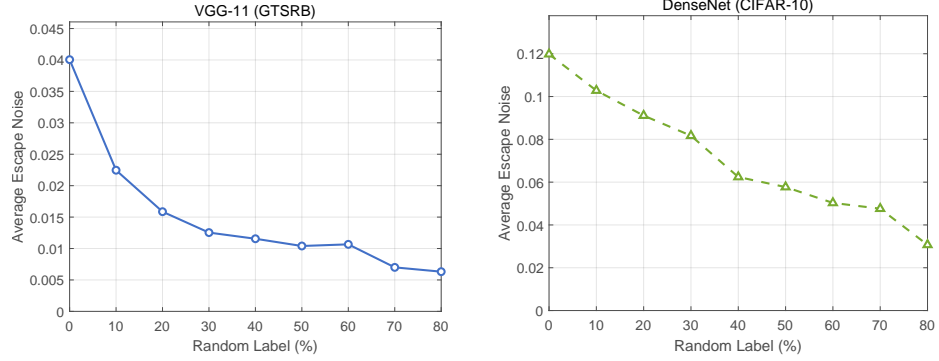


Figure 12: Average escape noise for models with different percentages of samples randomly labeled across two settings.

H Random-Label Ablations under Input and Parameter Perturbations

We report corresponding ablation experiments under input- and parameter-level perturbations, using the same datasets, architectures, and random-label settings.

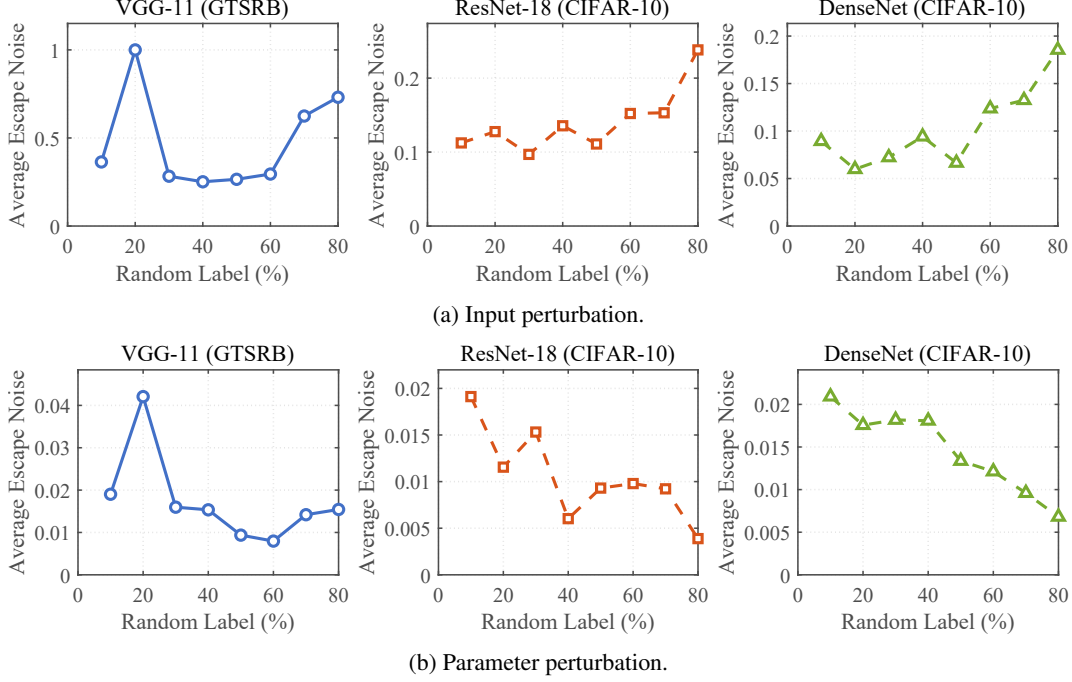


Figure 13: Average escape noise under different random-label ratios for *input-* (top) and *parameter-level* (bottom) perturbations. Experimental settings follow Figure 4. Neither perturbation exhibits a consistent monotonic decrease of escape noise as label randomness increases.

I Implementation Details of Input and Parameter Perturbations

We briefly describe the implementation of input- and parameter-level perturbations used in our experiments. To ensure a controlled comparison across perturbation mechanisms, we follow the same non-optimized, inference-time perturbation protocol used by APEX.

Input Perturbation. For input perturbation, we add i.i.d. Gaussian noise to the input image at inference time:

$$x' = \text{clip}(x + \sigma\epsilon, 0, 1), \quad \epsilon \sim \mathcal{N}(0, I),$$

where σ denotes the noise standard deviation.

Parameter Perturbation. For parameter perturbation, we add i.i.d. Gaussian noise to all floating-point parameters of the network:

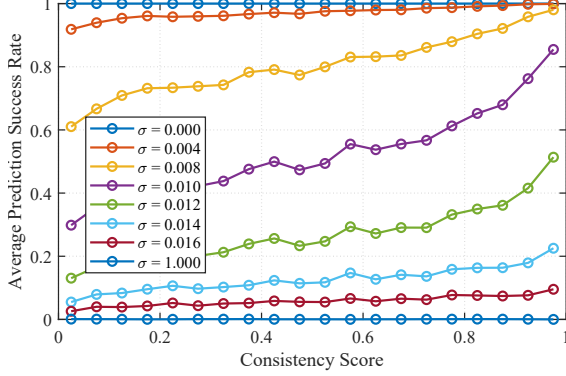
$$W' = W + \sigma\epsilon, \quad \epsilon \sim \mathcal{N}(0, I),$$

where the same σ is applied uniformly across layers. In all experiments, both perturbation types are non-optimized and applied independently across repeated evaluations.

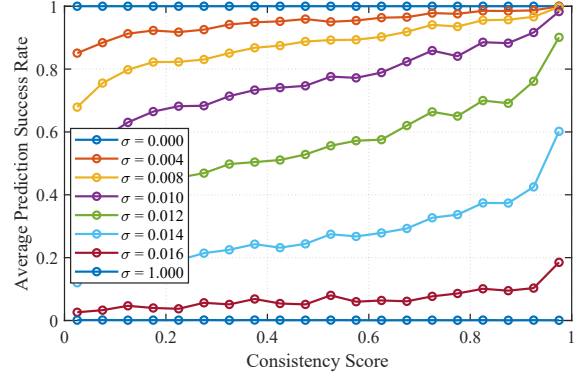
J Additional Results on Perturbation Stability and Sample Regularity

In the main text, we focus on activation perturbation as a general framework for probing sample regularity, and note that input perturbation constitutes a constrained special case. Here, we report corresponding input- and activation-level results across datasets and architectures to corroborate this relationship. The consistency score and memorization score form approximately complementary measures of sample regularity, satisfying $C\text{-score} + \text{Mem-score} \approx 1$ Jiang et al. [2021]. Therefore, we only report results in terms of C-score.

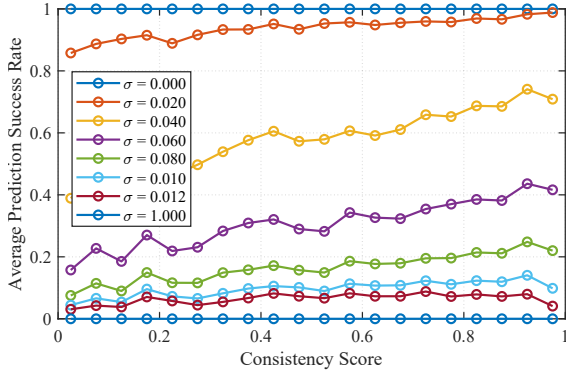
Specifically, we evaluate prediction stability under different noise magnitudes σ on ImageNet and CIFAR-100, with ResNet-50 and inception model respectively. All stability curves are obtained by averaging Monte Carlo prediction frequencies within bins of the corresponding regularity scores.



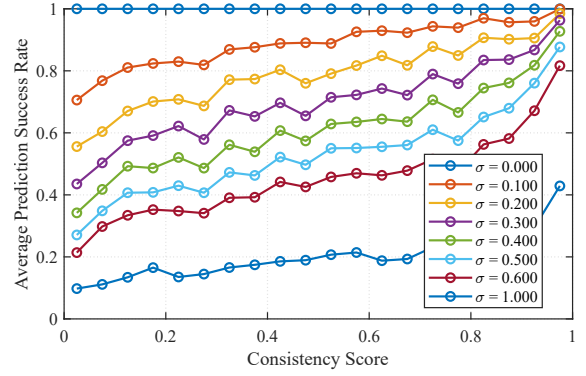
(a) CIFAR-100: activation perturbation stability.



(b) ImageNet: activation perturbation stability.



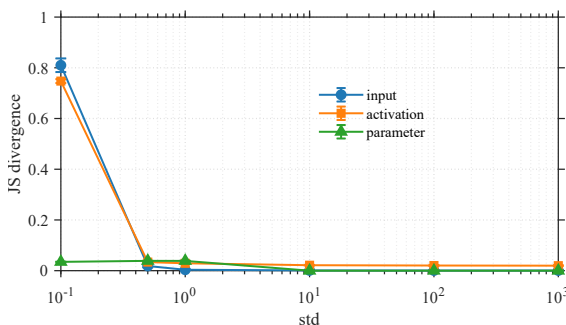
(c) CIFAR-100: input perturbation stability (constrained case).



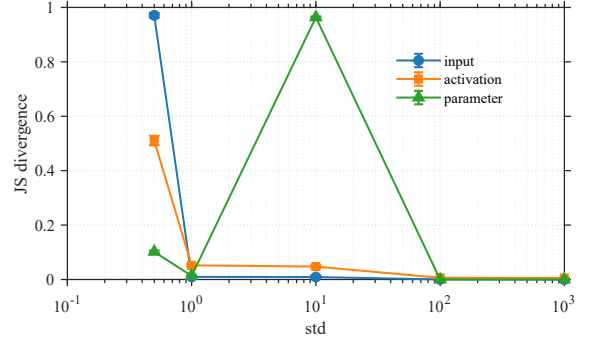
(d) ImageNet: input perturbation stability (constrained case).

Figure 14: Additional sample-level stability results on ImageNet and CIFAR-100. Top: activation perturbation, serving as the general framework. Bottom: input perturbation, corresponding to a constrained special case. Across datasets, prediction stability exhibits consistent correlations with consistency score, supporting the interpretation of escape noise as a reliable indicator of sample regularity.

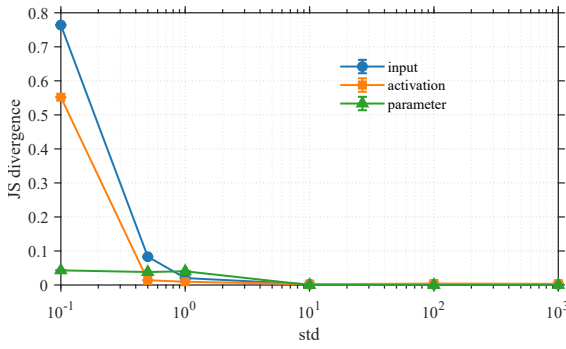
K Model-Level Output Distributions



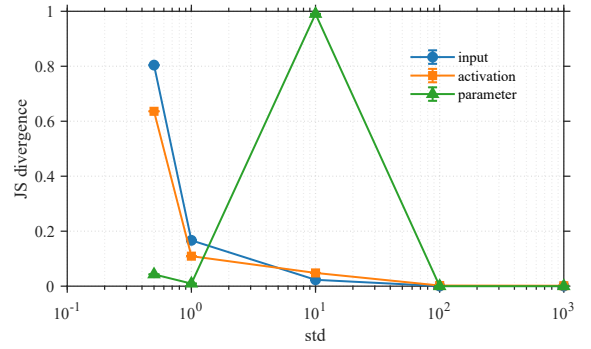
(a) JS divergence between output distributions from different inputs for ResNet-18 models.



(b) JS divergence between output distributions from consecutive noise magnitudes for ResNet-18 models.



(c) JS divergence between output distributions from different inputs for Inception models.



(d) JS divergence between output distributions from consecutive noise magnitudes for Inception models.

Figure 15: Jensen–Shannon (JS) divergence analysis of output distributions under large perturbations. **(Left Column)** Average pairwise JS divergence between output distributions obtained from different input samples at the same noise magnitude σ . **(Right Column)** JS divergence between the averaged output distributions at consecutive noise magnitudes. Experiments are conducted on CIFAR-100 with ten ResNet-18 models (top) and Inception models (bottom), using input-, activation-, and parameter-level perturbations. As σ increases, both metrics rapidly decrease toward zero, indicating convergence to a sample-independent and stationary output distribution. While all perturbation types exhibit this convergence, activation perturbation remains numerically stable and yields smoother transitions, whereas parameter perturbation becomes unstable under large noise.

L Backdoor Attack Configuration

All backdoor attacks in this paper are implemented using the BackdoorBox toolbox Li et al. [2023]. We adopt the *default configurations* provided by the toolbox for each attack, including trigger pattern, injection strategy, poisoning rate, and target-class assignment. No additional tuning or adjustments are applied. Visualization examples of backdoor triggers are shown below:

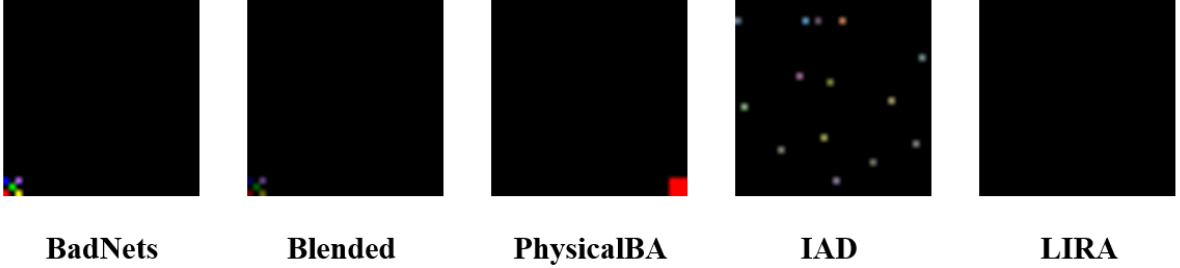


Figure 16: An example of backdoor triggers from five different attacks

M Transformers: Attenuated Global Collapse

Vision transformers are often reported to be more robust to out-of-distribution features, and backdoor triggers are known to behave similarly to OOD signals. If this robustness extends to the global representation structure, backdoored transformers may exhibit a weaker stationary output distribution collapse. As shown in Figure 17, backdoored DeiT models initially concentrate on the target class as noise increases, but partially re-disperse under larger perturbations. This behavior suggests that, in transformers, poisoned features distort local regions without fully dominating the global representation space, highlighting a limitation of collapse-based signals in this architecture.

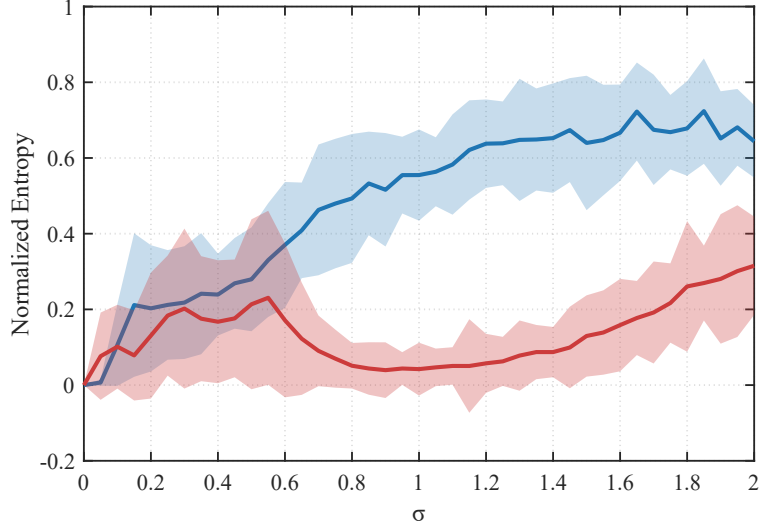


Figure 17: Average normalized entropy of benign and backdoored DeiT-small models under different noise standard deviations.

N Escape Noise Is Decoupled from Training Confidence

This appendix provides a detailed comparison between the evolution of escape noise and average softmax confidence over training epochs. While confidence increases monotonically as training progresses, escape noise remains largely stable, indicating that the two quantities capture distinct aspects of model behavior.

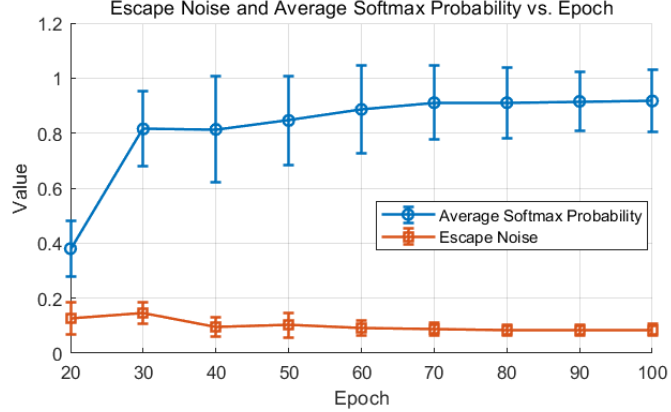


Figure 18: Average escape noise and average softmax probability vs. Epoch for 5,000 images sampled from CIFAR-10, with ResNet-18 model.

O Choice of Noise Type

While activation perturbation primarily uses Gaussian noise, it is not limited to this choice. We compared the KL divergence between output distributions under Gaussian, Laplace, and uniform noise. As shown in Figure 19, differences are minimal at high noise levels, suggesting that detection performance is largely determined by noise strength rather than its specific type.

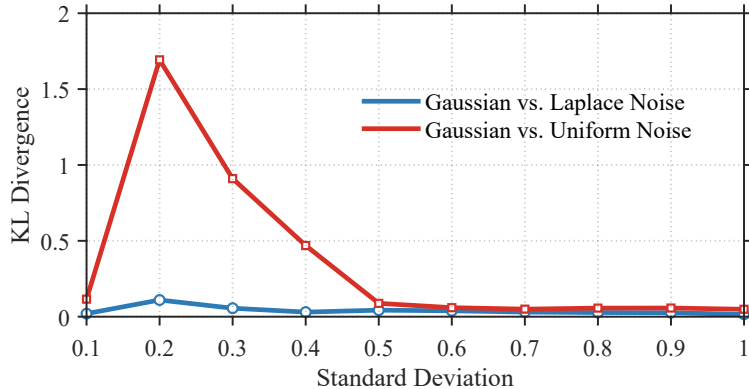


Figure 19: Average KL divergence between output distributions under Gaussian, Laplace, and uniform noise, averaged across ten ResNet-18 CIFAR-10 models.

P Single-Layer Activation Perturbation

Figure 20 shows that perturbing deeper layers results in higher output dispersion, indicating greater sensitivity in deeper layers. In backdoored models, the output is still concentrated on the target class throughout all layers.

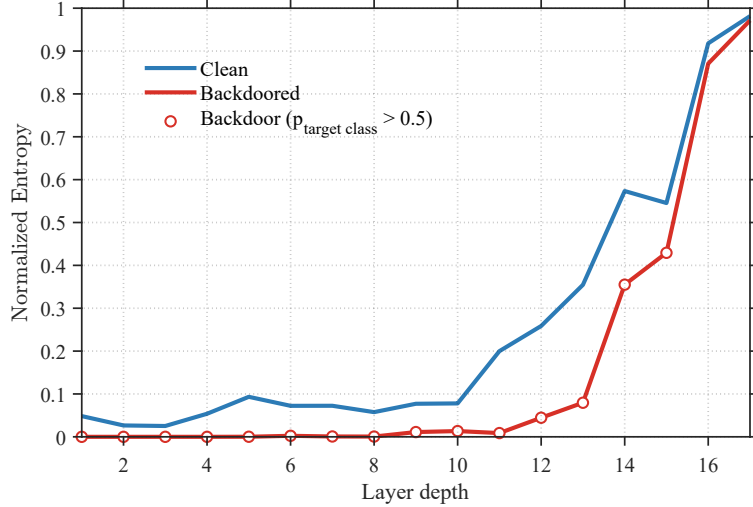


Figure 20: Average normalized entropy when injecting noise into a single ReLU layer for ten ResNet-18 models, CIFAR-100.

Q Activation Function Choice

To examine whether the stationary target-aligned behavior depends on the specific choice of activation function, we repeat the backdoor experiments using models trained with alternative nonlinearities on CIFAR-10. In addition to ReLU, we consider Leaky ReLU and GELU, which differ substantially in smoothness and negative-region behavior. For each model, we apply activation perturbation at inference time and measure the average probability assigned to the backdoor target class across Monte Carlo runs under increasing noise strength. Figure 21 reports the resulting target-class probabilities as a function of the noise standard deviation.

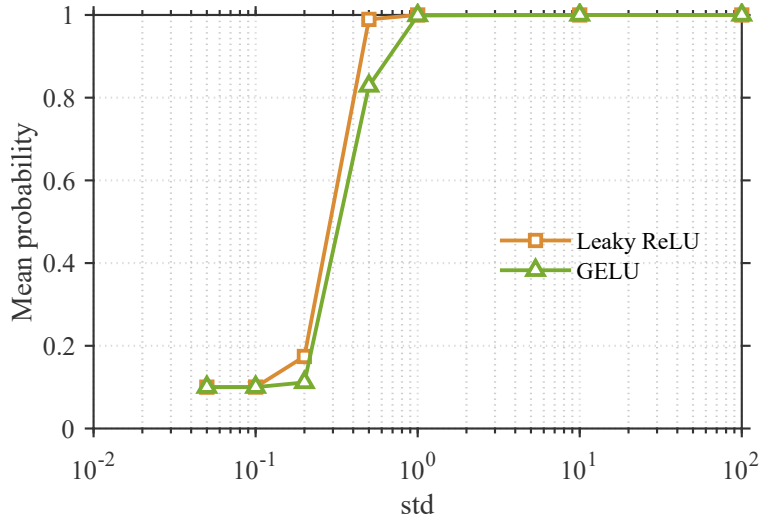


Figure 21: Average predicted probability of the backdoor target class under increasing activation noise for models trained with different activation functions. Both Leaky ReLU and GELU exhibit a sharp transition toward near-deterministic prediction of the target class, similar to ReLU-based models. This indicates that the observed stationary collapse is not specific to ReLU, but reflects a general property of activation perturbation.